



Article

How does globally accumulated tropical cyclone energy vary in response to a changing climate?

Kaiyue Shan ^a, Fengfei Song ^{b,c,*}, Yanluan Lin ^d, Wenchao Chu ^{d,e}, Chengfei He ^{f,g}, Pao-Shin Chu ^h, Lixin Wu ^{b,c}, Xiping Yu ^{i,*}

^a State Key Laboratory of Hydrosience and Engineering, Department of Hydraulic Engineering, Tsinghua University, Beijing 100084, China

^b Frontier Science Center for Deep Ocean Multispheres and Earth System and Physical Oceanography Laboratory, Ocean University of China, Qingdao 266100, China

^c Laoshan Laboratory, Qingdao 266100, China

^d Department of Earth System Science, Ministry of Education Key Laboratory for Earth System Modeling, Institute for Global Change Studies, Tsinghua University, Beijing 100084, China

^e Lamont-Doherty Earth Observatory, Columbia University, Palisades, NY 10964, USA

^f Rosenstiel School of Marine, Atmospheric, and Earth Science, University of Miami, Miami, FL 33149, USA

^g Woods Hole Oceanographic Institution, Woods Hole, MA 02543, USA

^h Department of Atmospheric Sciences, School of Ocean and Earth Science and Technology, University of Hawai'i at Mānoa, Honolulu, HI 96822, USA

ⁱ Department of Ocean Science and Engineering, Southern University of Science and Technology, Shenzhen 518055, China

ARTICLE INFO

Article history:

Received 13 July 2024

Received in revised form 3 December 2024

Accepted 4 December 2024

Available online 26 December 2024

Keywords:

Tropical cyclones

Accumulated cyclone energy

Interdecadal pacific oscillation

Climate change

Vertical wind shear

ABSTRACT

How tropical cyclone (TC) activity varies in response to a changing climate is widely debated. The accumulated cyclone energy (ACE) is one of the indicators of TC activity and has attracted considerable attention because of its close relationship with the damages caused by TCs. Previous studies have focused on detecting long-term trends in global ACE; however, the results are inconclusive. Here, it is revealed that the global ACE demonstrates a striking interdecadal variation over the past four decades, with a historical peak occurring in the 1990s. A close relationship between the interdecadal variability of the global ACE and the Interdecadal Pacific Oscillation (IPO) is also identified, with a Pearson correlation coefficient of 0.75 ($P < 0.01$). When the IPO is in its positive phase, more TCs with a longer lifetime occur owing to greater coverage of weak vertical wind shear (VWS) conditions over the tropics. The coverage of weak VWS conditions can be verified by either prescribing the observed sea surface temperature in atmospheric models or the observed IPO in coupled models, indicating the significant role of the IPO. Our findings show that the IPO affects the interdecadal variability of global TC activity through moderating atmospheric circulations.

© 2024 The Authors. Published by Elsevier B.V. and Science China Press. This is an open access article under the CC BY license (<http://creativecommons.org/licenses/by/4.0/>).

1. Introduction

The question of how global tropical cyclone (TC) activity could vary in response to a changing climate is important [1–8], as TC events are among the most devastating natural hazards occurring worldwide [9,10]. The accurate prediction of potential TC losses can be considered relevant to some integral metrics of TC activity [11]. An indicator among these metrics is the accumulated cyclone energy (ACE), which combines information on individual parameters, including number, intensity, and duration [12]. There is a statistically significant correlation between economic losses and ACE, even though this indicator does not account for whether TCs make

landfall, suggesting that years with high ACE have a greater overall potential for TC-related losses than years with low ACE [13].

Many studies have investigated the effect of long-term global warming on the number, intensity, and duration of TCs, however, the implications of the integral metrics are inconclusive due to the superposition of opposite contributions from these individual parameters [14]. Theoretical and numerical studies suggest decreasing frequency and increasing intensity in a warming climate [5,15,16]. A decrease in the global mean duration of intense TCs is observed, with an inverse relationship to the increase in intensity [17]. Although global climate models can provide physics-based simulations of Earth's climate, such models, in general, do not simulate TC activity accurately enough [18]. Most of the models under-resolve TCs [7], and there are large uncertainties in simulating atmospheric circulation that can influence TC activity [19,20]. Many efforts have been made to detect anthropogenic signals in TC activity over the historical period [4–6,21,22]. Since

* Corresponding authors.

E-mail addresses: songfengfei@ouc.edu.cn (F. Song), yuxp@sustech.edu.cn (X. Yu).

the introduction of geostationary weather satellites in the 1970s, TC observations have generally been considered accurate [6]. Based on satellite data, it was argued that the global ACE exhibited an increasing trend from the 1970s to the 2000s, highlighting the role of the warming ocean [1,2]. In contrast, a decreasing trend in global TC activity since the 1990s was shown [23]. The confidence in these detection analyses is relatively low, as the historical record may not be long enough to conclude any long-term trend, particularly in the presence of interdecadal variability [24–27].

Contradictory evidence on the trends in global TC activity during different subperiods may imply a possibility: global TC activity may be primarily influenced by interdecadal variability rather than a long-term trend. Previous research [28] has noted a historical low in global TC activity near the 2010s, but the possible reasons remain unclear. Note that the climate system is manifested not only by an increase in global average temperature but also by internal climate variability, e.g., the El Niño–Southern Oscillation on the interannual scale and the Interdecadal Pacific Oscillation (IPO) or Pacific Decadal Oscillation on the interdecadal scale [29,30]. There has been considerable effort from academic and government climate scientists to predict basin-wide statistics of TC activity, and the influence of internal climate variability on regional TC activity has been noted [26–27,31–33]. This raises questions about how global TC activity might exhibit interdecadal variations over the past few decades and whether these variations are related to low-frequency fluctuations in the climate system. Certain statistics of global TC activity have been shown to correlate with indices of internal climate variability [1,23,28,34]. However, the key mechanisms driving global TC activity, and whether these mechanisms are natural or anthropogenic, remain largely unexplored.

2. Data and methods

2.1. TC data

TC data are obtained from the International Best-Track Archive for Climate Stewardship version 4 [35]. TC data over the eastern North Pacific and North Atlantic basins are provided by the National Hurricane Center, and TC data over the remaining basins are provided by the Joint Typhoon Warning Center. The global best-track data since the 1980s are considered to be of high quality because geostationary satellites have been routinely used in monitoring TCs. The North Indian Ocean basin is excluded from the sample because there are few TC events. The best-track dataset provides estimates of TC intensity and position every six hours using measurements from *in situ*, radar, and satellite systems. To confirm the robustness of the findings, we have also examined another experimental TC dataset, i.e., ADT-HURSAT dataset [6], in which TC data are derived from satellite data for the period of 1979–2017 subsampled uniformly to 8 km horizontal resolution [36].

In the satellite era, an essential aspect of intensity estimation is to identify the presence of a TC eye in a satellite image. When a TC is in the weak stage of no eye scene, large uncertainty remains in estimating TC intensity. Additionally, the estimation of the TC duration in the weak stage is unreliable, as it depends on the absolute measures of TC intensity. Given that the TC eye generally appears when the TC has reached typhoon/hurricane intensity, our analysis only includes the TC events that reach at least typhoon/hurricane intensity (maximum sustained winds ≥ 64 knots or ≥ 33 m/s) during their lifetime. Excluding the data of TCs that do not reach typhoon/hurricane intensity to our analysis does not significantly alter our conclusions (Fig. S1 online).

There is considerable uncertainty in estimating TC intensity in both TC datasets when a TC is in the weak stage. The estimation

of the TC duration in the weak stage is also unreliable since it is based on absolute measures of TC intensity. Considering the poor quality of TC data during the weak stage, we entirely exclude periods in which TC events have not reached typhoon or hurricane intensity.

The ACE index convolves duration and intensity information for each individual TC around the globe [12]. Moreover, it is also used as a representative of TC energy available for ocean mixing or the size of TC-affected areas [37]. In general, the TC season in the Northern Hemisphere is defined as a continuous period of the calendar year, while the TC season in the Southern Hemisphere is defined as a continuous period from 1 July of the last calendar year to 30 June of the calendar year as the seasonal distribution of TC activity in the southern hemisphere straddles the calendar year. Such inconsistency between the two hemispheres is inadequate to investigate the variation in global TC activity. In this study, the 60-month running average of ACE (the mean value of the current month, the preceding 29 months, and the following 30 months) is calculated for each month, to eliminate the high-frequency variation in the time series of the ACE.

Before conducting the correlation analysis between the ACE index and climate mode time series, we detrended the global ACE time series based on the 1970–2019 period. To verify consistency, we calculated the global ACE correlation for both the 1970–2019 and 1981–2019 periods, obtaining similar results: a correlation of 0.75 ($P < 0.01$) with the IPO and 0.81 ($P < 0.01$) with VWS. In our results analysis, we focus primarily on the variation of global ACE during the 1981–2019 period.

As suggested by previous studies [28,31,38,39], there is an out-of-phase relationship of TC activity between the eastern North Pacific and North Atlantic basins. For a better understanding of the variations in eastern North Pacific/North Atlantic TCs [31,39] and for reducing the damage they cause [38], it would be better to consider both ocean basins together.

2.2. IPO index

The IPO is the dominant mode of interdecadal variability with an SST pattern similar to that of ENSO, and it is characterized by a ‘warm-tongue’ SST anomalies pattern with positive SST anomalies over the central and eastern parts of the tropical Pacific and negative anomalies over the western part of the Pacific in both hemispheres [40,41]. The IPO index is calculated based on the differences between the SST anomaly averaged over the central equatorial Pacific (10°S – 10°N , 170°E – 90°W) and the SST anomaly in the northwest (25° – 45°N , 140°E – 145°W) and southwest (50° – 15°S , 150°E – 160°W) Pacific [42].

2.3. GPI diagnosis

The GPI [43] is used to quantitatively determine the effect of environmental factors on the variations in TC genesis, which is expressed as

$$\text{GPI} = \left| 10^5 \eta \right|^{3/2} \left(\frac{H}{50} \right)^3 \left(\frac{V_p}{70} \right)^3 (1 + 0.1 \Delta V)^{-2} \quad (1)$$

where η is the absolute vorticity at 850 hPa ($/s$), H is the relative humidity at 700 hPa (%), V_p is the potential intensity (in terms of maximum wind; m/s), and ΔV (m/s) is the vertical wind shear between the horizontal winds at 200 hPa and 850 hPa levels. The potential intensity is obtained from sea surface conditions and vertical profiles of atmospheric conditions and the technical details of the calculation are available in Ref. [44]. The relative importance of the four environmental factors is assessed by calculating the anomalies of GPI using the values of one factor during the active

period while the other three environmental factors are fixed at their climatological values [45]. To further confirm the effect of VWS, a dynamic GPI [46] is applied, defined as follows:

$$\text{Dynamic GPI} = (2.0 + 0.1\Delta V)^{-1.7} \left(5.5 - 10^5 \frac{du}{dy}\right)^{2.3} (5.0 - 20\omega)^{3.4} \left(5.5 + \left|10^5 \eta\right|\right)^{2.4} e^{-11.8} - 1.0 \quad (2)$$

where ΔV and η are the same as in Eq. (1), ω represents the vertical wind velocity (Pa/s) at 500 hPa, u denotes the zonal wind (m/s) at 500 hPa, and $-du/dy$ represents the meridional shear vorticity (/s) associated with u . A detailed description of the DGPI computation can be found in Ref. [46,47].

2.4. VWS area index

Larger VWS could suppress TC genesis by disrupting the organized deep convection (the so-called ventilation effect), and vice versa [48]. VWS is calculated as the difference between the horizontal winds at 200 hPa and 850 hPa levels. The monthly mean wind fields with a horizontal resolution of $0.25^\circ \times 0.25^\circ$ are obtained from the European Centre of Medium-range Weather Forecasts Reanalysis v.5 (ERA5) global reanalysis [49].

Here, the area index of VWS is defined as the sum of areas in the tropical ocean (30°N – 30°S) where VWS is below a given threshold. The VWS area index time series remain highly consistent across different latitude bands as the VWS area index represents the area of low VWS values, which are primarily concentrated in the tropical ocean. The VWS of 4 m/s is used as the threshold in the definition of the VWS area index in this study. A sensitivity analysis is conducted to examine the robustness of this correlation relationship for different VWS thresholds (Fig. S2 online). It is suggested that the VWS area index can well explain the interdecadal variability of global ACE, with correlation coefficients of about 0.80 ($P < 0.01$) when the threshold of VWS is within the range of 3–8 m/s. The 60-month running mean values of the global ACE and VWS area index were calculated prior to performing the correlation analysis.

2.5. CMIP6 models

To estimate the relative contributions of anthropogenic warming and internal climate variability to the interdecadal variation in global ACE, we use the AMIP experiments and historical simulations from CMIP6 models [50]. The AMIP experiments are forced by the observed SST and sea ice concentration, and the CMIP6 historical simulations are derived by the coupled ocean–atmosphere models. CMIP6 models generally have coarse resolution and do not explicitly resolve TC dynamics. The VWS area index is used as a proxy of the interdecadal variation in global ACE, given that there is a close correlation between them (Fig. 1), with a correlation coefficient of 0.81 ($P < 0.01$). The VWS area index in model simulation results is calculated using the same definition and threshold as in observational data. The variables used to calculate the VWS area index include monthly horizontal winds at 850 hPa and 200 hPa. We produce a multi-model ensemble by averaging the simulations of 20 models with CMIP and AMIP simulations (Table S1 online).

To further isolate the role of IPO in the interdecadal variation of TC activity, we have estimated the VWS area index series based on the multi-model mean of the hist-resIPO experiments. The hist-resIPO experiment is a pacemaker-coupled historical climate simulation designed to isolate the impact of the IPO, which includes all forcings used in CMIP6 historical simulations and the observed historical SST restored in the tropical lobe of the IPO domain [51]. All available models with the outputs needed of the hist-resIPO

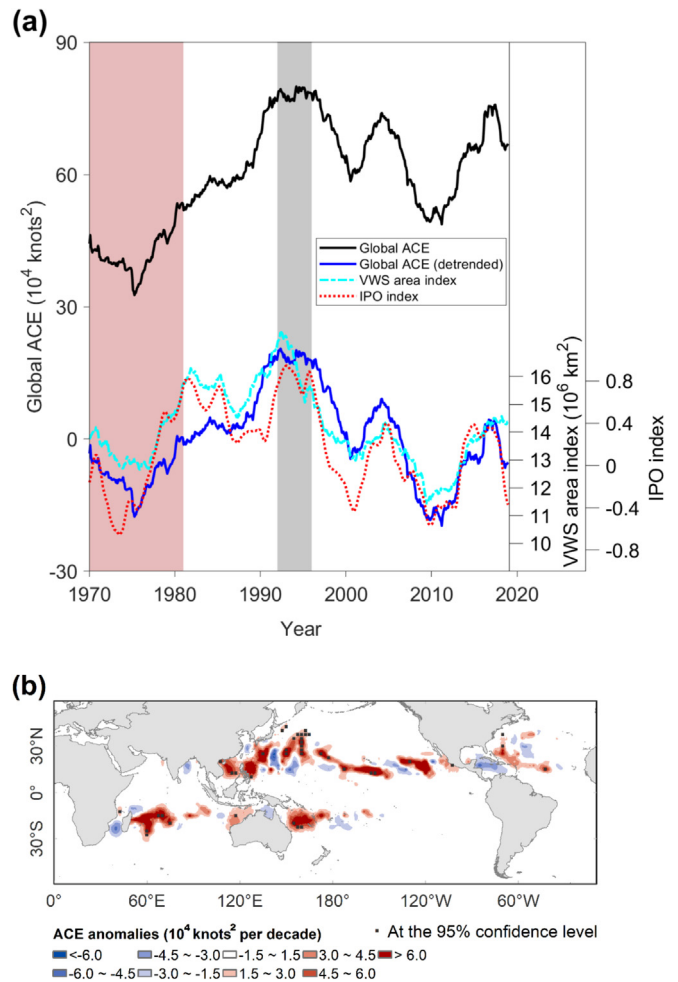


Fig. 1. Interdecadal variation in global ACE. (a) Time series of the 60-month running average of ACE for global TCs (black line) obtained from the best-track dataset for each month from 1970–2019; coherent variability of the detrended global ACE (blue solid line) with the IPO index (red dotted line; $R = 0.75$; $P < 0.01$) and the area index of the VWS (cyan dashed line; $R = 0.81$; $P < 0.01$). The 60-month running average of the IPO index and VWS area index are calculated. The grey belt represents the historical peak in the 1992–1996 pentad. The red shading represents data from before the 1980s, which is considered less reliable. (b) The anomalies of ACE with a $2.5^\circ \times 2.5^\circ$ grid in the boreal summer during June–October for the NH and boreal winter during December–April for the SH in the 1992–1996 pentad relative to the historical period of 1981–2019. The black squares indicate significance at the 95% confidence level.

experiments are used: FGOALS-f3-L (three realizations), FIO-ESM2-0 (one realization) and MRI-ESM2-0 (three realizations). The mean value of the realizations of each model is first obtained, and then the multi-model mean is calculated.

3. Interdecadal variation in the global ACE

Here, we consider global TC activity by analyzing ACE [12], which is defined in this study as the monthly sum of the squares of wind speeds for all TCs over a specific ocean basin or worldwide. Although satellite observations began in the 1970s, global coverage was only achieved by the 1980s, so we focus primarily on changes in global ACE since the 1980s. A striking interdecadal variation in the global ACE since the 1980s is observed. In Fig. 1a, the 60-month running average of the global ACE based on the best-track dataset [35] peaked in the 1992–1996 pentad and subsequently declined by approximately 40% from the late 1990s through the early 2010s. Then, the global ACE reached a low value near the

end of the 2010s. The low value of global ACE near the 2010s is consistent with previous research [28], which attributed this decline to large-scale climate modes such as the El Niño Southern Oscillation and the Pacific Decadal Oscillation. These findings suggest that global climate change during the past few decades, characterized by an indisputable warming trend in ocean temperatures [52,53], has not resulted in a directly detectable trend in global ACE. Furthermore, another metric, the power dissipation index [1] which is defined in a similar way but using the cube of the wind speed instead of the square (see Methods), also shows evident interdecadal variation (Fig. S3 online).

At the basin-wide scale (Fig. S4 online), the ACE in the pentad of 1992–1996 was approximately 25 % above average in the western North Pacific, South Pacific, and South Indian basins. In the eastern North Pacific and North Atlantic basins, which are considered as a whole due to their out-of-phase relationship with regard to TC activity [28,31,38,39], a local maximum of ACE in the 1992–1996 pentad is observed, approximately 10% above average. All major ocean basins contribute positively to the interdecadal variation in global ACE (Fig. 1b), demonstrating the robustness of this phenomenon. Notably, our results remain consistent regardless of the time window length (Fig. S5 online).

Although many previous studies have emphasized the effect of the IPO in moderating regional TC activity [31–33,54,55], how it affects global TC activity remains unknown. Here we examine whether the interdecadal variability of the global ACE is linked to the IPO. As shown in Fig. 1, the IPO underwent its positive phase at approximately the same time that the global ACE reached its historical peak. A strong correlation between the time series of the detrended global ACE (blue solid line) and the IPO index (red dotted line) is observed in Fig. 1a, with a correlation coefficient of 0.75 ($P < 0.01$). To further confirm the robustness of this correlation, TC data from 1981–2017 from the Advanced Dvorak Technique-Hurricane Satellite (ADT-HURSAT; see Methods) dataset were also used. The TC data of the ADT-HURSAT dataset are derived from satellite images with an 8 km horizontal resolution [6,36]. A statistically significant correlation is found between the interdecadal variability of global ACE obtained from the ADT-HURSAT dataset and the IPO index (Fig. S6 online). This consistency between the two datasets suggests that the relationship between the interdecadal variability of global TC activity and the IPO index is reliable.

4. Relative contributions from individual TC parameters

To understand the driving force behind the interdecadal variability of the global ACE, the relative contributions of individual TC parameters are examined. Note that ACE can be expressed as a multiplication of three statistical TC parameters: number, duration, and intensity [56]. As shown in Fig. 2, the time series of global TC number and duration display interdecadal variations, with a historical peak in the 1990s. Our findings align with previous studies suggesting that there is no clear evidence of a trend in global TC number due to the limited period of reliable TC observations and the influence of interdecadal variability [5,16,25,57]. While global warming has indeed caused TC tracks to shift poleward since the 1980s [58–60], this shift has not introduced a long-term trend in global TC duration. In contrast, TC intensity shows an upward trend with some fluctuations (Fig. 2). Additionally, we calculated the correlations between the IPO and variations in TC frequency, duration, and intensity, yielding correlation coefficients of 0.76 ($P < 0.01$), 0.56 ($P < 0.01$), and 0.17 ($P > 0.05$), respectively. These results suggest that TC frequency and duration may play a significant role in the influence of the IPO on global ACE.

Furthermore, we quantitatively assessed the relative contributions of individual TC parameters to the historical peak in global

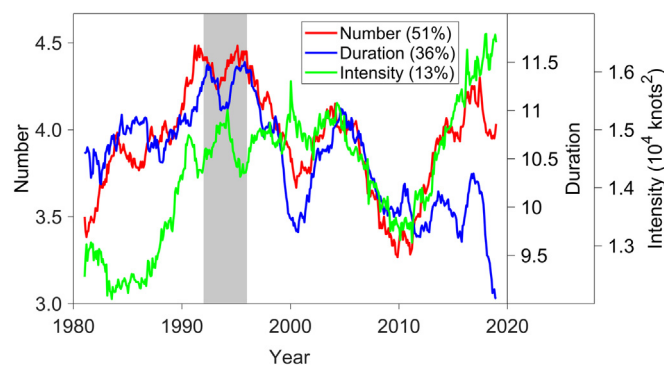


Fig. 2. Contribution of individual parameters to the interdecadal variation in the global ACE. Time series of the individual parameters of TCs, including number (red line), duration (blue line), and intensity (green line) obtained from the best-track dataset in each month from 1981–2019; the relative contribution of each parameter to the global ACE in the 1992–1996 pentad relative to the historical period of 1981–2019 is shown in brackets. The 60-month running averages of TC number, duration, and intensity are presented.

ACE during the 1992–1996 pentad. The relative contributions of TC number and duration to the historical peak in the global ACE in the 1992–1996 pentad are approximately 51% and 36%, respectively (jointly, accounting for around 87%). In contrast, TC intensity plays a relatively minor role, contributing around 13%. The robustness of these findings has been confirmed through a sensitivity analysis on the choice of typical periods (Table S2 online).

Given that the interdecadal variability of the global ACE is largely due to variations in TC number and duration, the variations in TC genesis density and track density may have to be paid attention. Focusing on the historical peak in the 1992–1996 pentad, one of the most prominent features of this interdecadal variation in the global ACE, it is found that the number of TCs that occurred in the 1992–1996 pentad increased over the central tropical Pacific and the eastern parts of other regions (Fig. 3a). A quantitative analysis indicates that the anomalies in TC genesis (Fig. S7 online) are largely responsible for the positive anomalies in TC track density (Fig. 3b). This result is not surprising. An anomalous increase in TC genesis number in the eastern part can lead to more TCs passing through the area, and TCs generated further east typically have a longer duration before encountering the continent or cold water [32,33,54].

5. The effect of the VWS

Next, we investigate the cause of TC genesis anomalies. Fig. 3c shows the anomalies of the genesis potential index (GPI) in the 1992–1996 pentad [43]. The anomalies of GPI could largely represent the characteristics of the observed variations in TC genesis density (Fig. 3a), despite regional inconsistencies in the western North Pacific and North Atlantic basins. The effects of the four individual factors involved in the GPI were assessed. As shown in Fig. 3d, the vertical wind shear (VWS) is the major contributor to the anomalies in the GPI, while little contribution is made by other factors (Fig. S8 online). A larger VWS could suppress TC genesis by disrupting organized deep convection, and vice versa [48]. The primary role of the VWS was confirmed (Fig. S9 online) when the dynamic GPI was used [46]. These results suggest that the VWS strongly controls TC genesis anomalies and thus the variation in the ACE.

To accurately illustrate the effect of the VWS on the interdecadal variability of the global ACE, an area index of the VWS is proposed, which is defined as the sum of areas where the VWS is below a given threshold. The time series of the VWS area index

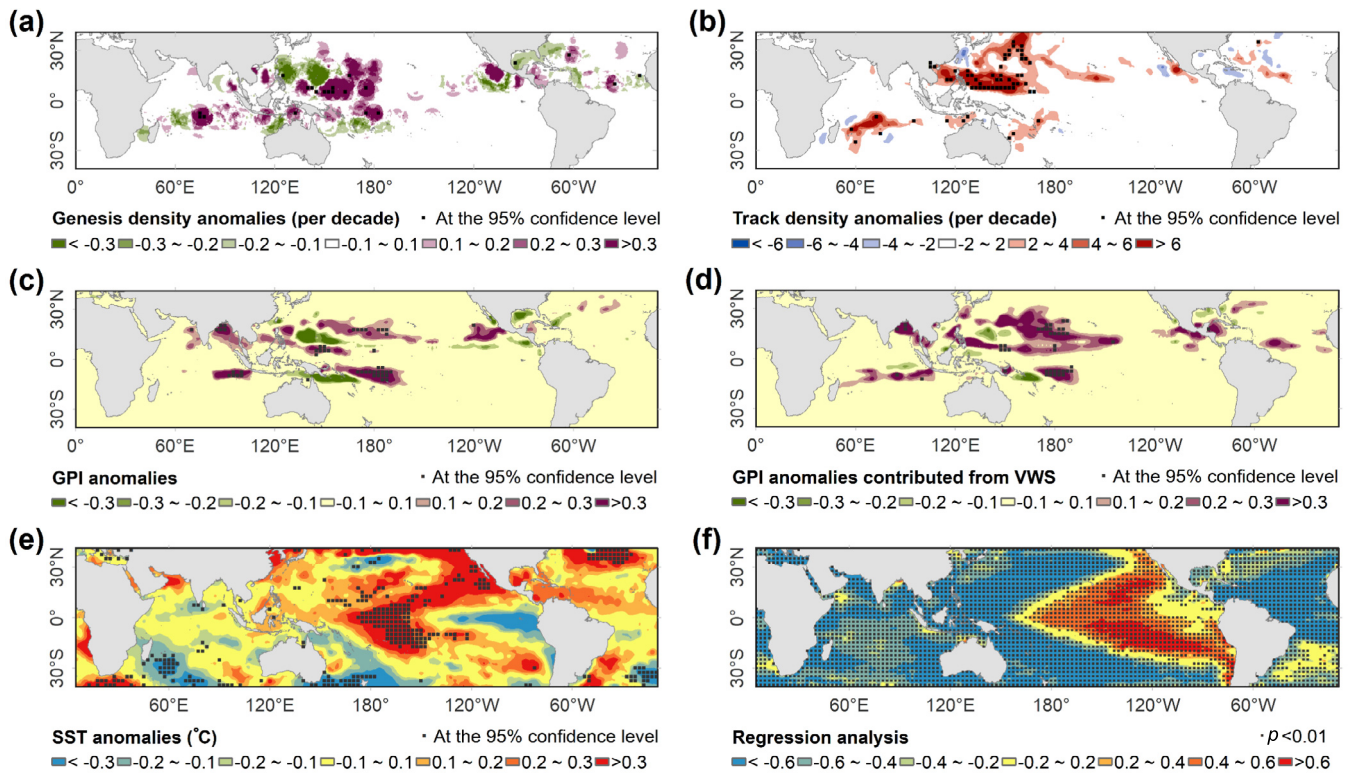


Fig. 3. TC genesis modulated by the IPO. The anomalies of (a) TC genesis density and (b) TC track density over a $2.5^{\circ} \times 2.5^{\circ}$ grid obtained from the best-track dataset in the boreal summer during June–October and boreal winter during December–April in the 1992–1996 pentad relative to the historical period of 1981–2019. The black squares indicate significance at the 95% confidence level. The anomalies of (c) the GPI calculated based on the ECMWF and ERA-5 datasets and (d) the GPI for varying VWS with other factors as climatology. (e) The anomalies of SST obtained from the ECMWF dataset. (f) Regression of the VWS area index onto the SST. The 60-month running average of the VWS area index and SST is calculated before the regression analysis.

(cyan dashed line in Fig. 1a) exhibits interdecadal variation that is highly consistent with the time series of the detrended global ACE derived from the best-track dataset (blue solid line in Fig. 1a), with a correlation coefficient of 0.81. This strong correlation between the VWS area index and interdecadal variability of the global ACE was also confirmed based on the ADT-HURSAT dataset (Fig. S6 online), with a correlation coefficient of 0.75 ($P < 0.01$). This relationship remains robust when different VWS thresholds are chosen (Fig. S2 online).

6. The role of the IPO

Variations in the VWS are closely related to changes in large-scale atmospheric circulation driven by the zonal gradient of SST. Coinciding with the decreased VWS over the central-eastern tropical Pacific in the 1992–1996 pentad (Fig. 3d), easterly wind anomalies at the 200 hPa level and westerly wind anomalies at the 850 hPa level along the tropical Pacific are observed (Fig. S10 online). A ‘warm tongue’ SST anomaly pattern was found in the 1992–1996 pentad, with positive anomalies over the central-eastern tropical Pacific and negative anomalies over the western part of the Pacific in both hemispheres, corresponding to a positive phase of the IPO (Fig. 3e). As a result, the zonal gradient of SST in the tropical Pacific was reduced, leading to a weakened Walker circulation, which is consistent with the observed easterly wind anomalies at the 200 hPa level and the westerly wind anomalies at the 850 hPa level (Fig. S10 online). The modest changes over the eastern North Pacific and North Atlantic basins could be explained by the influence of other climate modes, e.g., the Atlantic Multidecadal Oscillation as suggested in previous studies [38,39]. Many studies [10,33,61] have emphasized the role of the IPO in

affecting large-scale atmospheric circulation over the tropical Pacific. Recent modelling experiments revealed that the IPO could affect the variation in tropical Atlantic sea surface temperature remotely [62,63]. To further confirm the relationship between the variability of the VWS and the IPO, we regress the VWS area index onto the SST. The regression features warming over the central-eastern tropical Pacific and cooling in the western part of the Pacific (Fig. 3f), which resembles the positive IPO pattern.

To quantify the relative contributions of anthropogenic warming and internal climate variability to the interdecadal variability of global ACE over the past few decades, different kinds of experiments have been employed. Given the highly consistent relationship between the VWS area index and the interdecadal variation in the global ACE, we use the VWS area index as a proxy. The multi-model mean of historical simulations from twenty models of the Coupled Model Inter-comparison Project Phase (CMIP6) and Atmospheric Model Intercomparison Project (AMIP) experiments [50] from these models were calculated. The VWS area index calculated based on the AMIP simulations (blue line) can explain the interdecadal variability of the global ACE well, with a correlation coefficient of 0.78 ($P < 0.01$). In contrast, there is little correlation ($R = 0.02$; $P > 0.05$) between the detrended global ACE and VWS area index based on the multi-model mean of the CMIP simulations. When focusing on the models that can capture the relationship between the IPO and the VWS area index (Table S3 online), a similar conclusion can be drawn (Fig. S11 online): the VWS area index from the AMIP simulations explains the interdecadal variability of global ACE well. In contrast, the CMIP simulations perform poorly. These findings suggest that internal climate variability plays a significant role in moderating the interdecadal variability of global ACE over the past few decades.

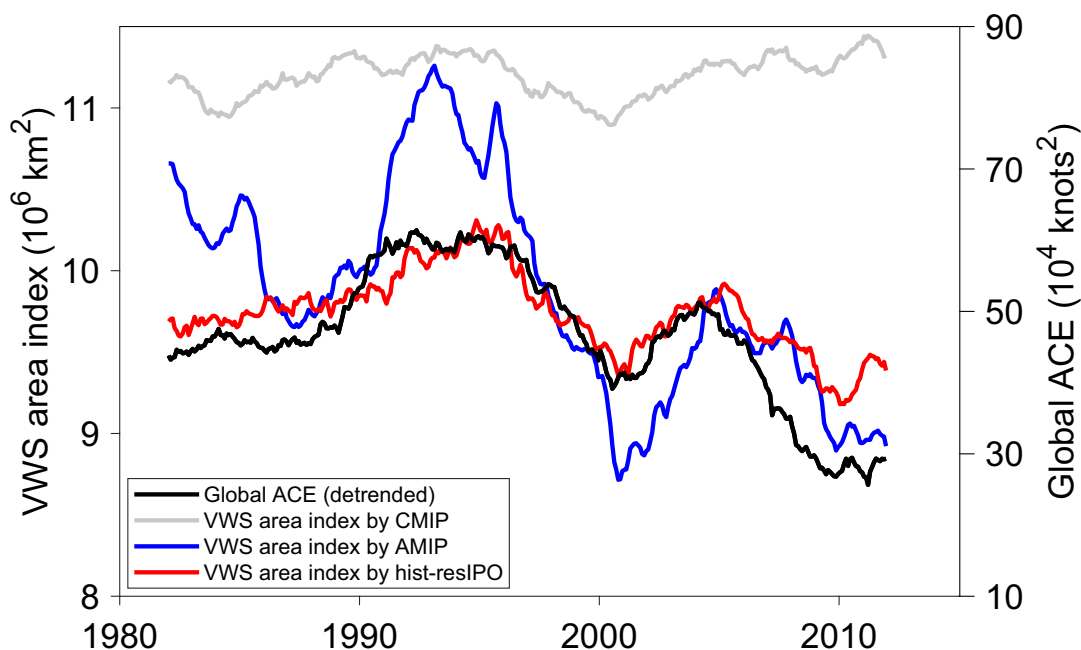


Fig. 4. Comparison of the simulated VWS area index and interdecadal variation in global ACE. Coherent variability between the detrended global ACE (black line) obtained from the best-track dataset for each month from 1981–2014 and the VWS area index calculated from the multi-model mean of the CMIP simulations (grey line; $R = 0.02$; $P > 0.05$), the VWS area index calculated from the AMIP simulations (blue line; $R = 0.78$; $P < 0.01$), and the VWS area index calculated from the hist-resIPO simulations (red line; $R = 0.91$; $P < 0.01$). The 60-month running mean values of the global ACE and VWS area index were calculated prior to performing the correlation analysis.

To isolate the role of the IPO, we estimated the VWS area index series based on the multi-model mean of the experiments that are forced by the observed IPO (hist-resIPO; see Methods). Based on the multi-model mean of the hist-resIPO experiments, there is a significant correlation between the detrended global ACE and VWS area index time series, with a correlation coefficient of 0.91 ($P < 0.01$). Additionally, the spatial distribution of VWS is well captured in the CMIP, AMIP, and hist-resIPO simulations, with spatial correlation coefficient $R > 0.90$ ($P < 0.01$) across all simulations (Fig. S12 online). This high spatial correlation across simulations confirms the meaningfulness of using the time series correlation coefficient for comparison. These findings further confirm that the IPO plays a crucial role in moderating the interdecadal variability of global TC activity.

7. Discussion

The globally averaged temperature has experienced a warming trend of $\sim 0.5^\circ\text{C}$ over the past four decades [52,53], whereas the global ACE has not exhibited trend-like variability, but rather distinct interdecadal variability, with a historical peak in the 1990s. Our analysis shows that the interdecadal variability of global ACE is closely related to the IPO, with a correlation coefficient of 0.75 ($P < 0.01$). The IPO in the positive phase boosts more TCs with a longer lifetime by causing a greater coverage of weak VWS conditions, thus increasing the global ACE, and vice versa. The newly introduced VWS area index calculated based on AMIP simulations can explain the interdecadal variability of the global ACE well, while CMIP simulations show poor performances. By calculating the time series of the VWS area index based on hist-resIPO experiments, the IPO is confirmed to play a crucial role in moderating the interdecadal variation in global TC activity. Although a previous study had suggested that the IPO may shift from its negative phase to its positive phase in the coming decades [30], the exact timing of the IPO phase transition remains uncertain. When the

IPO does shift to its positive phase, government officials, emergency managers, and the local community concerned must be well prepared to respond appropriately, as global TC activity could experience substantial enhancement, resembling levels observed in the 1990s.

Given the influence of the IPO on global TC activity, it is intriguing to discuss the underlying mechanism of its decadal evolution [64]. As recent research suggests [19,20,65], model bias in response to a given radiative forcing may be a major reason for the low confidence in the simulation results of the IPO, despite uncertainties in future emissions scenarios and internal climate variations. Many current climate models show that the SST in the tropical Pacific evolves to a more El Niño-like state against a greenhouse gas-induced warming, while observations show the opposite trend towards a more La Niña-like state [18]. Note that the tropical Pacific SST largely influences atmospheric circulation changes (e.g., VWS), and thus TC activity [10,33]. Here we discuss two possibilities: 1) the model bias in response to greenhouse gas warming could be considered random, and a meaningful simulation can be performed based on the multimodal mean; 2) most models incorrectly simulate the radiatively forced upper ocean warming pattern in the tropical Pacific, with similar error types and signs. If the model bias was considered to be random, it would contribute less to the discrepancy in the multi-model mean of the simulation results between the CMIP and AMIP simulations as shown in Fig. 4 of our study. Note that the internal variability is largely suppressed in the multi-model mean of the CMIP simulations, which, by contrast, is reflected in the multi-model mean of the AMIP simulations. That is, internal climate variability has dominated the evolution of the IPO over the past few decades and thus the interdecadal variability of global TC activity. In contrast, if there is a common model bias in simulating the radiatively forced upper ocean warming pattern in the tropical Pacific, its impact on the multi-model mean of the simulations is not negligible. Thus, the discrepancy between the CMIP and AMIP simulations may be induced by the model bias

and internal variability jointly. A recent study revealed that after removing the model bias of the tropical Pacific SST pattern, the interdecadal variation in tropical Atlantic SSTs was attributed to anthropogenic emissions and volcanic aerosols during the past few decades [66]. Similarly, we cannot rule out the possibility that the IPO may be partly affected by external forcings, but here we find that the IPO is a main driver of the interdecadal variability of global TC activity. Hence, confidence in future projections of TC activity relies on the level of scientific understanding of the physical mechanisms that affect the IPO.

Conflict of interest

The authors declare that they have no conflict of interest.

Acknowledgments

This research is supported by the National Natural Science Foundation of China (41961144014, and 42175029), and the Young Elite Scientists Sponsorship Program by China Association for Science and Technology (2023QNRC001).

Author contributions

Kaiyue Shan, Fengfei Song, and Xiping Yu designed the research. Kaiyue Shan performed the analysis and drew all the figures. Fengfei Song proposed the analysis of the CMIP6 model simulations. Kaiyue Shan wrote the first draft of the paper. All authors provided comments on different versions of the paper.

Data availability

TC best-track data are obtained from the IBTrACS (<https://www.ncei.noaa.gov/products/international-best-track-archive>). The ADT-HURSAT data are available from the Supporting Information in Ref. [6]. The ERA-5 reanalysis data are available at <https://cds.climate.copernicus.eu/>. SST data are obtained from the ERSSTv5 (<https://www.psl.noaa.gov/data/gridded/data.godas.html>). The raw outputs of CMIP6 models are available at <https://esgf-node.llnl.gov/search/cmip6/>.

Appendix A. Supplementary material

Supplementary data to this article can be found online at <https://doi.org/10.1016/j.scib.2024.12.036>.

References

- [1] Emanuel K. Increasing destructiveness of tropical cyclones over the past 30 years. *Nature* 2005;436:686–8.
- [2] Webster P, Holland G, Curry J, et al. Changes in tropical cyclone number, duration, and intensity in a warming environment. *Science* 2005;309:1844–6.
- [3] Sobel A, Camargo S, Hall T, et al. Human influence on tropical cyclone intensity. *Science* 2016;353:242–6.
- [4] Shan K, Lin Y, Chu P, et al. Seasonal advance of intense tropical cyclones in a warming climate. *Nature* 2023;623:83–9.
- [5] Knutson T, Camargo S, Chan J, et al. Tropical cyclones and climate change assessment. Part1: detection and attribution. *Bull Am Meteorol Soc* 2019;100:1987–2007.
- [6] Kossin J, Knapp K, Olander T, et al. Global increase in major tropical cyclone exceedance probability over the past four decades. *Proc Natl Acad Sci USA* 2020;117:11975–80.
- [7] Emanuel K. Limitations of reanalyses for detecting tropical cyclone trends. *Nat Clim Chang* 2024;14:143–5.
- [8] Zhao J, Wang F, Zhan R, et al. How does tropical cyclone genesis frequency respond to a changing climate. *Geophys Res Lett* 2023;50:e2023GL102879.
- [9] Mendelsohn R, Emanuel K, Chonabayashi S, et al. The impact of climate change on global tropical cyclone damage. *Nat Clim Change* 2012;2:205–9.
- [10] Shan K, Yu X. Variability of tropical cyclone landfalls in China. *J Clim* 2021;15:9235–47.
- [11] Klotzbach P, Chavas D, Bell M, et al. Characterizing continental US hurricane risk: which intensity metric is best. *J Geophys Res* 2022;127:e2022JD037030.
- [12] Hemmati M, Camargo S, Sobel A. How are Atlantic basin-wide hurricane activity and economic losses related. *Environ Res Climate* 2022;1:021002.
- [13] Bell G, Halpert M, Schnell R, et al. Climate assessment for 1999. *Bull Am Meteorol Soc* 2000;81:S1–S50.
- [14] Kang N, Elsner J. Trade-off between intensity and frequency of global tropical cyclones. *Nat Clim Chang* 2015;5:661–4.
- [15] Knutson T, Camargo S, Chan J, et al. Tropical cyclones and climate change assessment Part II: Projected response to anthropogenic warming. *Bull Am Meteorol Soc* 2020;101:E303–22.
- [16] Zhao H, Zhao K, Klotzbach P, et al. Decreasing global tropical cyclone frequency in CMIP6 historical simulations. *Sci Adv* 2024;10:eadi2142.
- [17] Wang S, Rashid T, Throp H, et al. A shortening of the life cycle of major tropical cyclones. *Geophys Res Lett* 2020;47:e2020GL088589.
- [18] Sobel A, Lee C, Bowen S, et al. Near-term tropical cyclone risk and coupled Earth system model biases. *Proc Natl Acad Sci USA* 2023;120:e2209631120.
- [19] Seager R, Henderson N, Cane M. Persistent discrepancies between observed and modeled trends in the Tropical Pacific Ocean. *J Clim* 2022;35:4571–84.
- [20] Wills R, Dong Y, Proistosescu C, et al. Systematic climate model biases in the large-scale patterns of recent sea-surface temperature and sea-level pressure change. *Geophys Res Lett* 2022;49:e2022GL100011.
- [21] Shan K, Yu X. Enhanced understanding to poleward migration of tropical cyclone genesis. *Environ Res Lett* 2020;15:104062.
- [22] Wang S, Murakami H, Cooke W. Anthropogenic effects on tropical cyclones near Western Europe. *npj Clim Atmos Sci* 2024;7:173.
- [23] Klotzbach P, Wood K, Schreck III C, et al. Trends in global tropical cyclone activity: 1990–2021. *Geophys Res Lett* 2022;49:e2021GL095774.
- [24] Landsea C. Hurricanes and global warming. *Nature* 2005;436:686–8.
- [25] Murakami H, Delworth T, Cooke W, et al. Detected climatic change in global distribution of tropical cyclones. *Proc Natl Acad Sci USA* 2020;117:10706–14.
- [26] Zhao J, Zhan R, Wang Y, et al. Contribution of Interdecadal Pacific Oscillation to the recent abrupt decrease in tropical cyclone genesis frequency over the western North Pacific since 1998. *J Clim* 2018;31:8211–24.
- [27] Zhao J, Zhan R, Wang Y, et al. Untangling impacts of global warming and Interdecadal Pacific Oscillation on long-term variability of North Pacific tropical cyclone track density. *Sci Adv* 2020;6:eaba6813.
- [28] Maue R. Recent historically low global tropical cyclone activity. *Geophys Res Lett* 2011;38:L14803.
- [29] Kosaka Y, Xie S. Recent global-warming hiatus tied to equatorial Pacific surface cooling. *Nature* 2013;501:403–7.
- [30] Dai A, Fyfe J, Xie S, et al. Decadal modulation of global surface temperature by internal climate variability. *Nat Clim Change* 2015;13:555–9.
- [31] Li W, Li L, Deng Y. Impact of the interdecadal Pacific oscillation on tropical cyclone activity in the North Atlantic and Eastern North Pacific. *Sci Rep* 2015;5:12358.
- [32] Lin I, Chan J. Recent decrease in typhoon destructive potential and global warming implications. *Nat Commun* 2015;6:7182.
- [33] Shan K, Yu X. Interdecadal variability of tropical cyclone genesis frequency in Western North Pacific and South Pacific Ocean basins. *Environ Res Lett* 2020;15:ab8093.
- [34] Wang B, Yang Y, Ding Q, et al. Climate control of the global tropical storm days (1965–2008). *Geophys Res Lett* 2010;37:L07704.
- [35] Knapp K, Kruk M, Levinson D, et al. The international best track archive for climate stewardship (IBTrACS) unifying tropical cyclone data. *Bull Am Meteorol Soc* 2010;91:363–76.
- [36] Bhatia T, Vecchi G, Knutson T, et al. Recent increases in tropical cyclone intensification rates. *Nat Commun* 2019;10:635.
- [37] Shi R, Zhang Q, Xu F, et al. Decreasing trend of tropical cyclone-induced ocean warming in recent decades. *Environ Res Lett* 2023;18:064013.
- [38] Wang C, Wang L, Wang X, et al. North-south variations of tropical storm genesis locations in the Western Hemisphere. *Geophys Res Lett* 2016;43:367–74.
- [39] Gong Z, Liu Y, Sun C, et al. Linking AMOC variations with the multidecadal seesaw in tropical cyclone activity between eastern North Pacific and Atlantic. *J Geophys Res* 2021;126:e2021JC017308.
- [40] Power S, Casey T, Folland C, et al. Inter-decadal modulation of the impact of ENSO on Australia. *Clim Dyn* 1999;15:319–24.
- [41] Folland C, Renwick J, Salinger M, et al. Relative influences of the interdecadal Pacific oscillation and ENSO on the South Pacific convergence zone. *Geophys Res Lett* 2002;29:21–1–4.
- [42] Henley B, Gergis J, Karoly D, et al. A triple index for the interdecadal Pacific oscillation. *Clim Dyn* 2015;45:3077–90.
- [43] Emanuel K, Nolan D. Tropical cyclone activity and global climate, 26th Conf. on hurricanes and tropical meteorology, Miami, FL, *Amer Meteor Soc* (2004), pp. 240–241.
- [44] Bister M, Emanuel K. Low frequency variability of tropical cyclone potential intensity 1. Interannual to interdecadal variability. *J Geophys Res*, 2002;107:ACL 26-1-ACL 26-15.
- [45] Camargo S, Emanuel K, Sobel A. Use of a genesis potential index to diagnose ENSO effects on tropical cyclone genesis. *J Clim* 2007;20:4819–34.
- [46] Murakami H, Wang B. Patterns and frequency of projected future tropical cyclone genesis are governed by dynamic effects. *Commun Earth Environ* 2022;3:77.

- [47] Wang B, Murakami H. Dynamic genesis potential index for diagnosing present-day and future global tropical cyclone genesis. *Environ Res Lett* 2020;15:114008.
- [48] Tang B, Emanuel K. A ventilation index for tropical cyclones. *Bull Am Meteorol Soc* 2012;93:1901–12.
- [49] Hersbach H, Bell B, Berrisford P, et al. The ERA5 global reanalysis. *Quart J R Met Soc* 2020;146:1999–2049.
- [50] Eyring V, Bony S, Meehl G, et al. Overview of the coupled model intercomparison project phase 6 (CMIP6) experimental design and organization. *Geosci Model Dev* 2016;9:1937–58.
- [51] Zhou T, Turner A, Kinter J, et al. Overview of the global monsoons model intercomparison project (GMMIP). *Geosci Model Dev* 2016;9:3589–604.
- [52] Trenberth K, Fasullo J, Balmaseda M. Earth's energy imbalance. *J Clim* 2014;27:3129–44.
- [53] Karl T, Arguez A, Huang B, et al. Possible artifacts of data biases in the recent global surface warming hiatus. *Science* 2015;348:1469–72.
- [54] Song J, Klotzbach P, Duan Y. On the relationship between western North Pacific tropical cyclone accumulated cyclone energy and the Pacific–North American pattern. *Int J Climatol* 2022;42:6373–83.
- [55] Cai Q, Chen W, Chen S, et al. Recent pronounced warming on the Mongolian Plateau boosted by internal climate variability. *Nat Geosci* 2024;17:181–8.
- [56] Emanuel K. Environmental factors affecting tropical cyclone power dissipation. *J Clim* 2007;20:5497–509.
- [57] Sobel A, Wing A, Camargo S, et al. Tropical cyclone frequency. *Earth's Future* 2021;9:e2021EF002275.
- [58] Kossin J, Emanuel K, Vecchi G. The poleward migration of the location of tropical cyclone maximum intensity. *Nature* 2014;509:349–52.
- [59] Sharmila S, Walsh K. Recent poleward shift of tropical cyclone formation linked to Hadley cell expansion. *Nat Clim Chang* 2018;8:730–6.
- [60] Song J, Klotzbach P. What has controlled the poleward migration of annual averaged location of tropical cyclone lifetime maximum intensity over the western North Pacific since 1961. *Geophys Res Lett* 2018;45:1148–56.
- [61] Hsu P, Chen K, Tsou C, et al. Future Changes in the frequency and destructiveness of landfalling tropical cyclones over East Asia projected by high-resolution AGCMs. *Earth's Future* 2021;9:e2020EF001888.
- [62] Meehl G, Hu A, Castruccio F, et al. Atlantic and Pacific tropics connected by mutually interactive decadal timescale processes. *Nat Geosci* 2021;14:36–42.
- [63] Yao S, Chu P, Wu R, et al. Model consistency for the underlying mechanisms for the inter-decadal Pacific Oscillation-tropical Atlantic connection. *Environ Res Lett* 2022;17:124006.
- [64] Boer G, Smith D, Cassou C, et al. The Decadal Climate Prediction Project (DCPP) contribution to CMIP6. *Geosci Model Dev* 2016;9:3751–77.
- [65] Sun W, Li J, Yu R, et al. Exploring changes of precipitation extremes under climate change through global variable-resolution modeling. *Sci Bull* 2024;69:237–47.
- [66] He C, Clement A, Kramer S, et al. Tropical Atlantic multidecadal variability is dominated by external forcing. *Nature* 2023;622:521–7.
- [67] Yokoi S, Takayabu Y. Attribution of decadal variability in tropical cyclone passage frequency over the western North Pacific: A new approach emphasizing the genesis place of cyclones. *J Clim* 2013;26:973–87.